# Clinical Considerations for a Minimally Invasive Wireless EEG System

By

Akshit Chhabra

Sc.B, Brown University, 2023

Thesis

Submitted in partial fulfillment of the requirements for the Degree of Master of Science in the School of Engineering, and the Center for Biomedical Engineering at Brown University

PROVIDENCE, RHODE ISLAND

MAY 2024

This thesis by Akshit Chhabra is accepted in its present form by the School of Engineering, and the Center for Biomedical Engineering as satisfying the thesis requirements for the degree of Master of Sciences

Date 04/18/2024

Prof. Arto Nurmikko, Advisor

Recommended to the Graduate Council

Date 04/25/2024

Prof. David Berson, Reader

Date 04/30/2024

Prof. Marissa Gray, Reader

Approved by the Graduate Council

Date 04/30/2024

Prof. Marissa Gray, Biomedical Engineering Master's Program Director

## AUTHORIZATION TO LEND AND REPRODUCE THE THESIS

**As the sole author of this thesis, I authorize Brown University to lend it to other institutions or individuals for the purpose of scholarly research.**

Date 04/18/2024

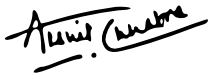

Akshit Chhabra, Author

**I further authorize Brown University to reproduce this thesis by photocopying or other means, in total or in part, at the request of other institutions or individuals for the purpose of scholarly research.**

Date 04/18/2024

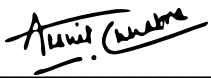

Akshit Chhabra, Author

**Acknowledgements**

First, I would like to thank my thesis advisor, Professor Arto Nurmikko, for allowing me to work as part of his lab and for his constant support throughout my research. I would like to thank Dr. Ah-Hyoung Lee for sharing her microfabrication and electronics expertise and helping with key aspects. I would like to thank Dr. Lee and Dr. Jihun Lee, whose subdermal EEG project this work builds on. I would also like to thank my thesis committee - Prof. David Berson and Prof. Marissa Gray for agreeing to be readers of the thesis and providing valuable feedback. I would like to thank Ning Zhang, doctoral candidate at the Nurmikko lab, for his help with 3D printing and the optical bench setup. I would like to thank Prof. Andras Zsom for helping me learn machine learning. I would like to thank Aanchal Sheth for her help with storing key samples and with visualizations. Finally, to all my friends and family - this would not have been possible without your support.

**Table of Contents**

**List of Tables**

**List of Illustrations**

## Background

Electroencephalography (EEG) is a medical imaging technique that reads electrical activity generated within brain structures. The activation of neurons leads to the generation of local current flows and creates electrical dipoles between the soma and the apical dendrites. Sensors called electrodes are able to detect these minute changes in electric potential, amplify them, and display them in a format that can be read by trained professionals [1]. EEG imaging can read normal as well as abnormal brain activity, making it a very powerful diagnostic and monitoring tool in clinical neurology. One very important application of EEG is for the diagnosis and care of patients with various forms of epilepsy.

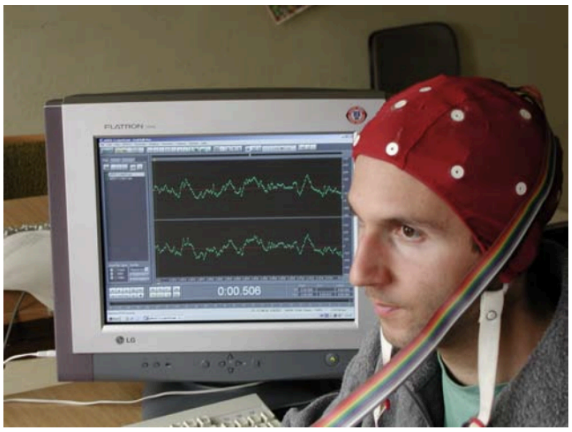


***Figure 1:*** *Conventional scalp EEG setup [2].*

Epilepsy is a disorder of the brain characterized by an enduring predisposition to generate epileptic seizures [3]. These seizures or ictal events can be debilitating for patients and can occur at any time without any notice. Current methods of epilepsy monitoring rely on conventional surface EEG, where a cap of electrodes is placed over clinically defined regions on the scalp, as shown in Fig. 1. This works well in the short-term, when the patient is in a clinical or ambulatory setting. However, the fact that it cannot be used for more than a few days, forms a significant limitation. This is because the inter-ictal time interval can range from minutes to years [4].

Without capturing the ictal EEG recordings, clinicians often have to rely on inter-ictal abnormalities called inter-ictal epileptiform discharges (IEDs) to form a diagnosis and proceed with treatment options. The association of IEDs with seizure frequency and severity is variable at best and an absence of IEDs cannot rule out a diagnosis of epilepsy [5]. Further, normal stressors experienced in daily life that cause these abnormalities may not be replicated in a monitored and artificial setting [6]. However, taking this "cap" of electrodes outside the clinical setting has its own challenges. EEG signals are on the scale of microvolts and therefore, maintaining a good signal to noise ratio while not disrupting daily activities is very tough [7]. Even if that were to happen, patients are often reluctant to wear a bulky cap due to stigmatization.

At the other end of the EEG spectrum is intracortical EEG, where depth electrodes are surgically implanted directly onto brain regions [8]. This provides reliable and accurate EEG data about the origins of the seizure or the epileptogenic zone but carries with it the dangers and risks associated with brain surgery. The realistic time duration of this method is even shorter and therefore, its use is limited to intraoperative and intensive care monitoring [9].

Thus, we identified a need for an accurate, reliable, and chronic monitoring method of brain activity that does not disrupt everyday activities for epilepsy patients. In an ideal scenario, patients would benefit with 24/7 continuous, long-term monitoring of their brain activity that does not hinder their daily life but still allows doctors to intervene as early as possible in the event of any abnormality. The Nurmikko Lab is making this a reality in the form of a highly miniaturized, wireless, minimally invasive subdermal EEG probe strip [10]. In this thesis, I take the work of the lab forward by looking into certain clinical considerations before the device is ready to be deployed. The first is a method of insertion of the probe that is quick, convenient, and minimally invasive for the physician to perform, easy and efficient to scalably manufacture,

and considerate of the delicate and complex microelectronics. Next, since the data generated by this ultra long term device would be enormous, I develop a computationally efficient automated seizure detection aid for clinicians using machine learning.

### 1.1 Subdermal EEG

Recently, subcutaneous or subdermal EEG has been recognized as a promising method for long-term epilepsy monitoring. The idea is for the probes to go beneath the scalp, thereby, reducing skin attenuation and resulting in better signal to noise ratios with lesser electrical artifacts [11]. Essentially, the proximity to brain tissue leads to a more reliable recording and in theory, if the implant is biocompatible and does not lose its recording efficiency, it can remain sub-scalp for ultra-long extended periods of time ranging from several months to even a few years. Outside of our lab, there have been two prominent efforts to construct a subdermal EEG system - one from the Danish company UNEEG [12], and the other from a group of researchers at the University of Melbourne [13]. Both devices center an approach with a ~10 cm long subcutaneous strip inserted from behind the ear, with leads to a separate electronic amplifier/radio module that is held in a subcutaneous pouch behind the ear, making them rather invasive. Both devices have only one or two sensing electrodes and scaling them to a larger number seems to be difficult. UNEEG's device is undergoing clinical trials and preliminary data suggests signal quality comparable to a singular scalp electrode. However, to get good coverage of the brain, scaling up is required.

The device being developed at our lab, by Drs. Ah Hyoung and Jihun Lee, aims to achieve this [14]. Our design (schematic shown in Fig. 2) consists of upto a 10cm long and 1mm wide polyimide strip with four (and scalable to 10-12) metal (eg. Pt or Au) electrodes. These

electrodes connect to a customized ultrasmall EEG recording application-specific integrated circuit (ASIC) for brain signal capture and radio frequency (RF) transmission. The system-on-chip ASIC integrates the circuit components required for (i) wireless energy harvesting, EEG recording, (ii) data communication and (iii) multi-chip networking functions by leveraging current semiconductor technology. Both the power delivery to the microchips and the transmission of the EEG signals takes place via transcutaneous inductive coupling, configurable in the 500 MHz - 1 GHz frequency range. Polyimide (PI), as a material, provides the flexibility to navigate the contours of the scalp. With the PI thickness of 100 micrometers, the overall thickness of the device can be kept down to 0.3mm, making it compatible with hypodermic needles and thus, a minimally invasive insertion. The lab has validated the strip's ability to record microvolt-size EEG signals in-vitro and multiple strips can be inserted to achieve brain coverage scalability. Currently, work is ongoing to fabricate hermetic sealing methods for chronic implantation and to further improve recording capabilities in the low frequency range, leveraging the lab's previous expertise [14]. The work of this thesis builds on these previous achievements in order to seamlessly integrate our device into a clinical setting.

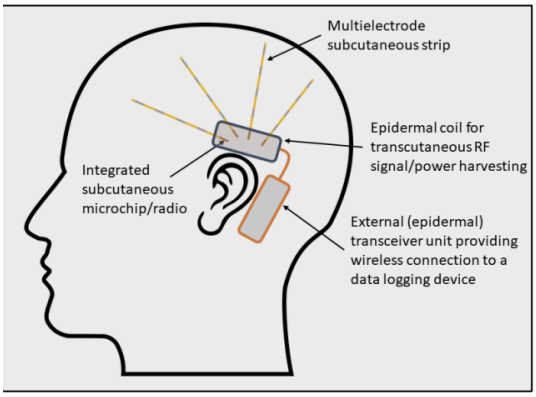


***Figure 2**: Proposed schematic of implanted wireless multichannel EEG device.*

The first of these clinical considerations is a method of insertion of the device that stays true to its minimally invasive nature, is easy and intuitive for the clinician to conduct, does not

damage the device, and is quick and efficient to scalably manufacture. Currently used insertion methods in devices like the one created by UNEEG involve pushing a custom needle through a blunt dissection and holding the implant in place using another atraumatic tool while the needle is retracted [15]. Not only does this require a wider incision to use the atraumatic tool, but the tool could also potentially damage the implant during the procedure. The tool is not sold as part of the device package and therefore, leaves room for error. To comply with all the afore-mentioned design requirements, I developed a novel method consisting of a bioresorbable polyethylene glycol barb-like microstructure that provides temporary hardening of the polyimide strip, so that it does not bend or damage during insertion, adheres to the subcutaneous fat layer upon insertion, and allows for the one custom hypodermic needle to be removed with the strip still in place without the need for any additional invasive tools. The needle can then be reused if multiple strips are to be inserted.

### 1.2 Machine Learning for Seizure Detection

The second clinical consideration was regarding the vast amount of data that would be generated by a longitudinal, ultra long term EEG device. It would be ideal to find a way to automate the seizure detection process, not intended to replace the clinician, but to serve as an aid. Machine learning has long been used for this purpose and has achieved good accuracy scores [16]. The machine learning pipeline for seizure detection consists of four steps: data collection, data preparation, applying machine learning classifiers and performance evaluation. Since our device is not clinically ready yet, data collection for this thesis was done using publicly available open source data. There are plenty of data repositories that researchers have used, including the Children's Hospital Boston, Massachusetts Institute of Technology EEG dataset (CHB-MIT)

[17], the Freiburg EEG dataset [18], and what was used for this thesis - the Bonn University EEG dataset [19]. This dataset comprises five subsets, where each one denoted as (A–E) contains 100 single-channel recordings, and each of them has a 23.6 s duration, captured by the international 10–20 electrode placement scheme [20]. All the signals are recorded with the same 128-channel amplifier system channel.

This data, however, is raw, and to make any sense of it, one needs to perform extensive feature extraction. Features can be extracted in the time domain, the frequency domain, and through transforming the data using Discrete Wavelet Transforms (DWT), Continuous Wavelet Transform (CWT), and Fourier Transform (FT). Some examples of extracted features used in the literature are shown in Table 1 [21].

Once feature extraction is complete, the data is ready for a machine learning classifier to be applied. In this case, the problem is a binary classification problem, where a data point can either be classified as a “seizure” or as “baseline”. Previously, multiple classifiers have been applied for seizure detection, including basic logistic regression, decision tree based models like random forests, and black box models like support vector machines (SVMs) and K Nearest Neighbors (KNN) [22]. Deep learning models like artificial neural networks (ANN) have also been applied [23] but for the purposes of this thesis, I only focus on machine learning methods.

The classifiers work on the data and provide predictions. The way to evaluate how well the model is performing is through its accuracy of prediction. Using accuracy in a straightforward manner, especially in clinical datasets, is not that relevant because it does not indicate the amount of false positives and false negatives, which are of paramount importance when it comes to diagnosing seizures [24]. Thus, the more important metric, used in this thesis as well, is the F1 score, where false-positives and the false-negatives are taken into account.

Performance of models on the Bonn University EEG dataset in the literature has ranged from 95.6% to 100% [25] [26]. More details about the exact equations for the F1 score and the different features and models used are given in Section 3.1.

Applying these classifiers on extremely large datasets is computationally expensive and time consuming. It is very important to understand how these models are working in order to optimize them but machine learning methods have been notorious for their black box nature and lack of interpretability [27]. Here, I use a novel decision tree based algorithm XGBoost and extract feature importances from it. Using these feature importances, I narrow down the top five features and rerun the model with only those features instead of all of the extensive data. This results in almost a 50% reduction in computational time without significantly compromising on model performance. Going ahead, this will be invaluable for an ultra long term, continuous monitoring device.

| **Feature extraction methods** | **Relevant features** |
|---|---|
| Time-domain features | Mean, variance, mode, median, skewness, kurtosis, max, min, zero crossing, line length, energy, power, Shannon entropy, sample entropy, approximate, entropy, fuzzy entropy, hurst exponent, standard deviation |
| Frequency-domain features | Spectral power, spectral entropy, energy, peak frequency, median frequency |
| Time–frequency-domain features | Line length, min, max, Shannon entropy, approximate entropy, standard deviation, energy, median, root mean square |
| Discrete Wavelet Transformation (DWT) | Bounded variation, coefficients, energy, entropy, relative bounded, variation, relative power, relative scale energy, variance, standard deviation |
| Continuous Wavelet Transformation (CWT) | Energy's standard deviation, energy, coefficient z-score, entropy |
| Fourier Transformation (FT) | Median frequency, power, peak frequency, spectral entropy power, spectral edge frequency, total spectral power |

***Table 1:*** *Commonly used feature extraction methods and features for EEG signal datasets [21].*

**Insertion Technique**

To make a subdermal implant truly unobtrusive and minimally invasive, the insertion technique is of paramount importance. In talking with clinicians, we identified a few considerations that would have to be met in order for this device to have widespread adoption. Firstly, the procedure should be able to be done under local anesthesia with a small incision behind the ear. The hypodermic needle used should be comparable to current standards - around 15 gauge or ~1.8mm in diameter [15]. The procedure should be intuitive to conduct without requiring extensive training sessions for the clinician. It should have a high rate of success and if multiple strips need to be inserted, the same apparatus should be able to be used. Apart from these, there are engineering considerations. The strip has delicate and complex electronics and microchips. The procedure should not be damaging to any of these. Polyimide was chosen as the material for the strip because of its flexibility, therefore, any insertion method should accommodate this flexibility. In the following section, I describe the design iterations and process to fully meet all of these requirements.

**2.1 Materials and Methods**

To begin the insert tool design process, I had to find the smallest diameter hypodermic needle that could fit our device. By simply trying needles ranging from 13 gauge to 21 gauge, I found that in order to guide the strip into the needle effortlessly, 13 gauge was the smallest we could do. In needles bigger than that, some amount of forceful shoving was required, which could potentially damage the strip. However, 13 gauge needles are not particularly minimally invasive. I realized that the thickness of our strip was much smaller than its width. Therefore, if a machine press was used to flatten the hypodermic needle to a rectangular cross-section, a smaller

diameter needle could be used by increasing its width and decreasing its height. By using a hydraulic press at the Brown University Joint Engineering and Physics Instrument Shop, I was able to custom flatten a 15 gauge needle (Frigid Fluid Co.$^{TM}$) to perfectly fit our subdermal EEG strip, as shown in Fig. 7b. The needle was 15 cm long, so it could well accommodate our 10 cm long strip.

Now that we had a customized hypodermic needle, the next step was to figure out how to keep the strip in place as the needle was removed post-insertion. Building off the UNEEG device, I started off with using an atraumatic 20 gauge needle to hold the strip in place as I removed the 15 gauge needle. While the procedure seemingly worked, an atraumatic needle not only added an additional required component, but also left damaging marks on the strip. Therefore, we needed to find a better alternative.

That is when the inspiration from facelift threads struck. Threads used in facelift procedures have barb-like structures running across them [28]. These barbs do not oppose motion in the direction that they face but when one tries to pull them out, they tug on to surrounding structures, thereby keeping the implants in place. This would be ideal in our case where the barb would adhere to the subdermal skin and keep the strip in place as the needle is extracted. I decided to use polyethylene glycol (PEG, Sigma Aldrich Co.) as the material for the barb, providing two benefits. First, the barb would be hardened and would provide the PI strip some temporary strength and stiffness during the insertion procedure. And second, it would be bioresorbable, dissolving after some time in the bodily environment, preserving the strip's flexibility in the long term and also making the extraction procedure easier with no barb present.

The first step in producing these PEG barb microstructures was to make a mold where I could insert the strip and get it covered in PEG of the desired shape. To do so, I proceeded with

computer aided design in Fusion 360. The files were then sent to an Elegoo Mars 3D printer, which produced a resin-based mold. The print was washed with isopropyl alcohol (IPA) for ten minutes to clean it, cured under ultraviolet (UV) light for ten minutes, and then cured at 125℃ for 5 hours to solidify completely. These ideal parameters were found after multiple prints where the molds still had contaminants or liquid resin remaining. The mold CAD design is shown in Fig. 4a with a successful draft analysis, indicating good mold release. The physical mold is shown in Fig. 4b.

With the mold ready, the PI strip could be inserted in it, covered with the desired material, and then removed with the covering on top. For initial testing, I used polydimethylsiloxane (PDMS, SYLGARD™) instead of PEG. PDMS is a material frequently used in research in and as molds [29] and would provide a proof of concept that barb formation and adhesion to the PI strip was actually possible. I used a standard 1:10 curing agent to base elastomer ratio, and vacuum degassed it to remove any air bubbles. I put the PDMS on top of the strip in the mold and removed the excess using a blade. It was then cured at 100°C overnight. The PDMS barbs showed good formation (pictured in Fig. 4c) and the learnings from this test included avoiding any air bubbles in the coating mixture and to use anti-adhesive mold release spray (Mann Release Technologies) on the 3D printed mold beforehand to ensure that the barbs do not have more adhesion to the mold than the strip itself and can be removed easily. The entire workflow is shown in Fig. 3.

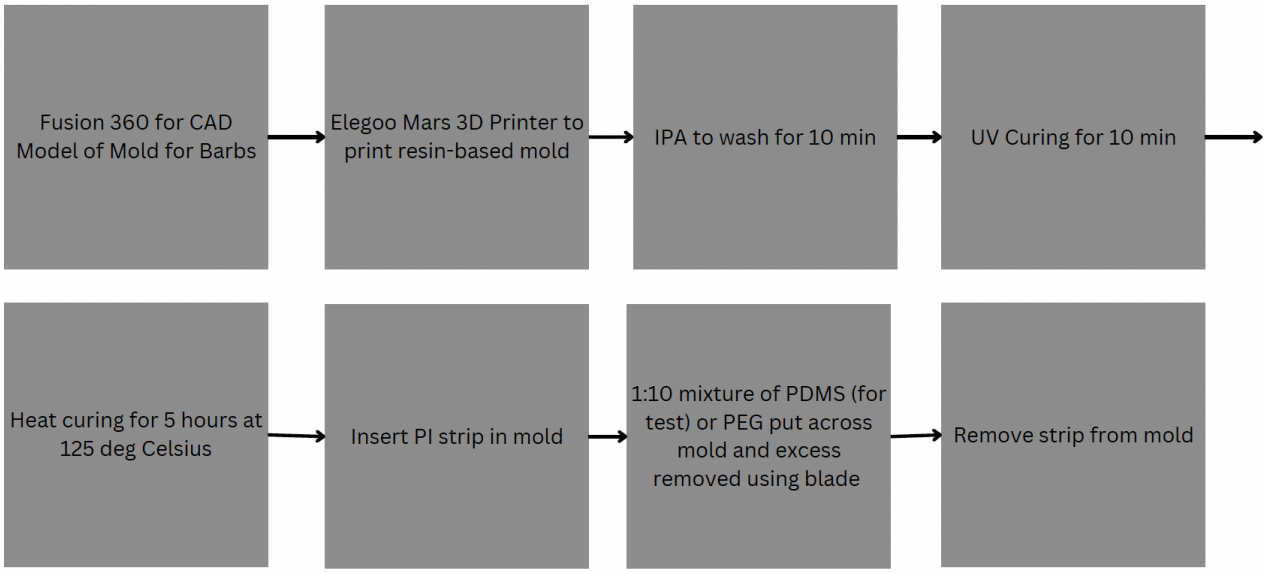


***Figure 3:*** *Workflow for fabrication of PEG barb microstructure.*

Using PEG next presented its own challenges. High temperatures >40℃ are needed to melt PEG crystals into a liquid form that can be poured over a mold. At the same time, vacuum degassing is required to remove air bubbles. If the PEG went below 40℃, it would recrystallize. Therefore, the PDMS protocol was modified to do quick alternating cycles of heating and vacuum degassing for 2 minutes each and repeating for a total of 3 times. To optimize the heating cycles, a hot plate was used on the bottom, and a heat blower on top. Excess PEG was again removed using a blade. Overall, by the end of all iterations, the PEG barbs (Fig.4d) could be produced on a PI strip in under 15 minutes.

The first PEG strip iteration started with multiple barbs lining the entire length of the strip (Fig. 4e). While this granted a lot of structural support to the PI strip, it also took away from its flexibility and ability to navigate the contours of the scalp. The next iteration was with alternating 2 cm segments of PEG barbs and bare PI strip (Fig. 4f). Some amount of flexibility was regained but compromises had to be made on the quality of the barbs and the time it took to make this type of strip - 5 times more than the previous method because the strip needed to be

inserted and removed from the mold 5 different times to create barbs at 5 different places. Further, with the additional width added by the barbs - 0.5mm on each side, we would need to find a larger needle, again defeating the minimally invasive purpose we began with.

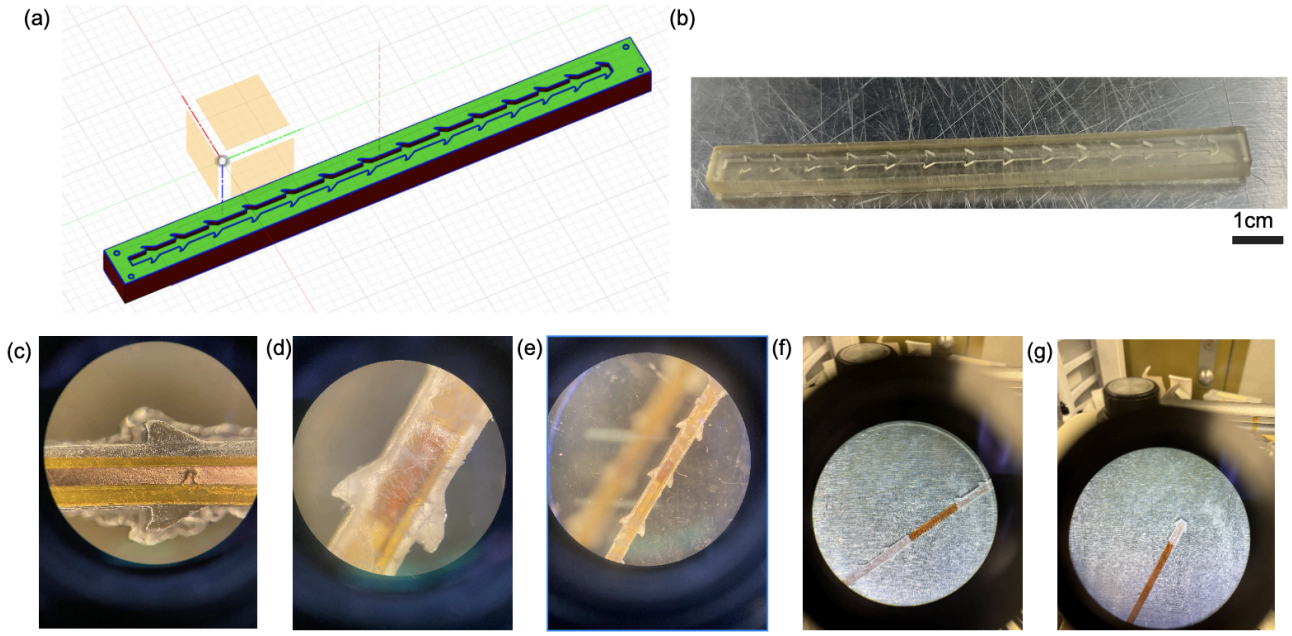


***Figure 4:*** *Design Evolution: (a) CAD mold with draft analysis; (b) 3D printed resin mold that PI strip can be inserted in; (c) test barb using PDMS; (d) PEG barb; (e) strip covered with multiple barbs; (f) strip with alternating barbed and bare regions; (g) final design with singular barb at one end.*

Therefore, a singular barb at one end was chosen as the final design (Fig. 4g). This was not only quick and easy to produce (<15 min), but because the barb stayed outside the needle (perfect placement shown in Fig. 6c), a 15 gauge needle could still be used. To test and validate this technique of insertion, I created a dermis phantom. Using values from previous literature [30], this included 24% gelatin from porcine skin (Type A porcine powder, Sigma-Aldrich, Corp., MO, USA), 1 % agar (A1296 powder, Sigma-Aldrich), and 75% distilled water. I also wanted to test how much force was required to remove the strip after insertion, i.e., how strong the PEG barb adhesion was, as well as how fast the PEG dissolution was. So, I used a digital

newton meter, attached to the PI strip using an alligator clip to pull the strip out and note down force values at different time intervals. This was first done manually and then automated using an optical bench stage. The automated stage moved at a speed of 5 mm/s. The setup is shown in Fig.8a. The results of these tests are presented in the following section.

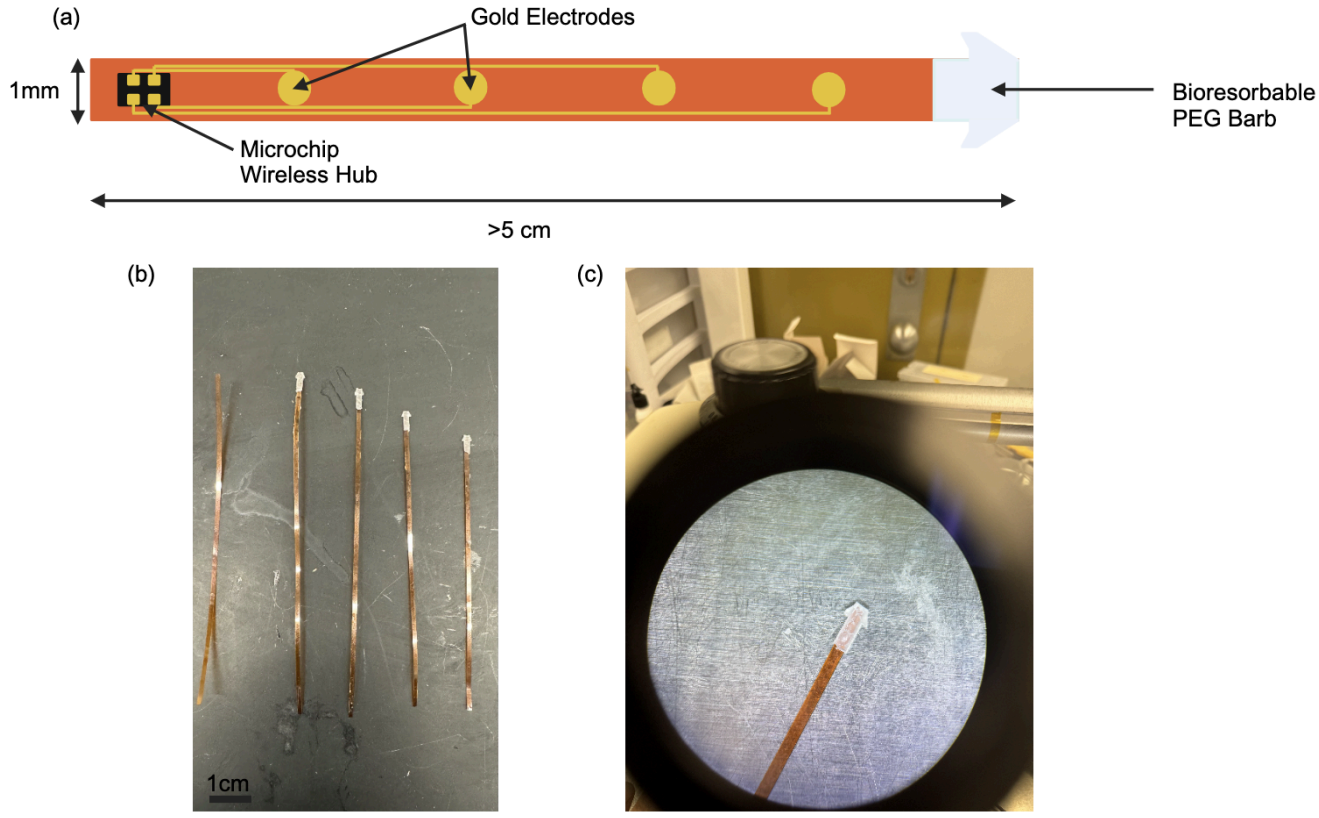


***Figure 5:*** *(a) Schematic of the wireless EEG recording strip (sample with 4 electrodes) with a bioresorbable polyethylene glycol barb on one end; (b) Strips of various sizes (7 to 10 cm) with barbs and one control; (c) Singular barb under a microscope.*

## 2.2 Results and Discussion

Having gone through multiple design iterations, the finalized insert tool consisted of a custom-pressed 15 gauge hypodermic needle into which the PI strip can be inserted easily. The other end of the strip has a singular bioresorbable PEG barb that provides additional temporary

strength to the strip during insertion and then dissolves for easy extraction. The PEG barb is also designed in a way that it does not oppose the insertion motion but adheres strongly to subcutaneous skin layers when it is pulled upon in the opposite direction. This ensures that the strip is held in place when the hypodermic needle is pulled out. The strip schematic and images are shown in Fig. 5. The integration of the barbed strip with the hypodermic needle is shown in Fig. 6. The entire schematic of insertion is shown in Fig. 7.

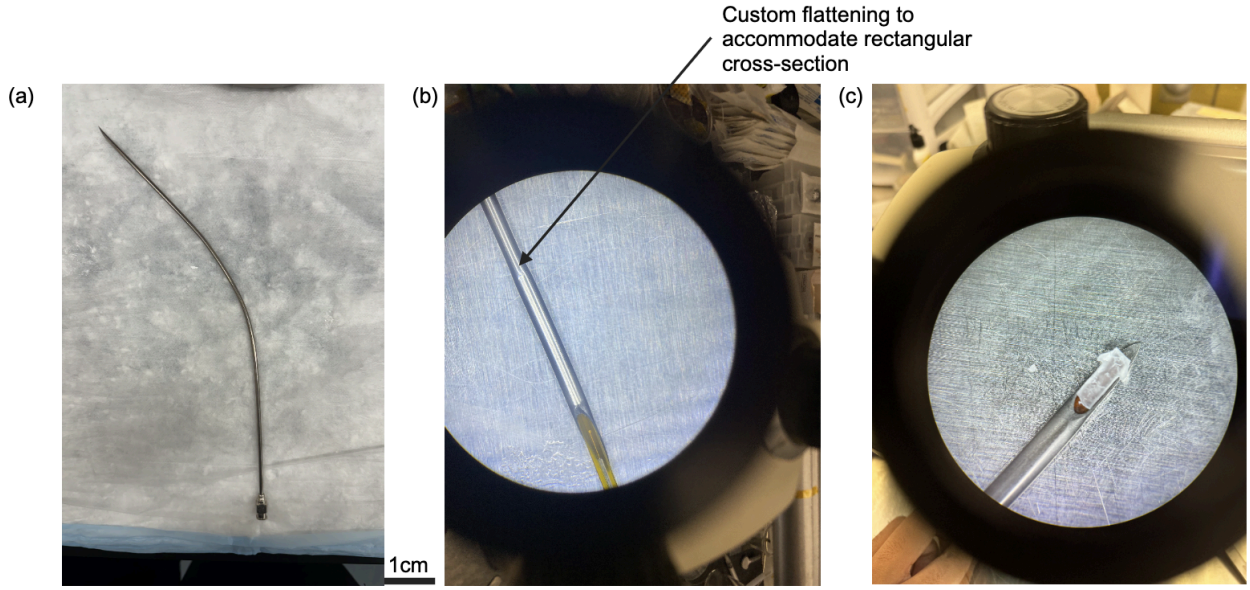


***Figure 6:*** *(a) Extra long, flexible 15 gauge hypodermic needle to hold 10 cm strip; (b) custom machine pressing to help the strip fit into the needle; (c) perfect strip placement with the barb with needle tip still exposed.*

The procedure is intuitive for the clinician by simply inserting the needle with the strip inside, tunneling through the subdermal scalp space, and extracting the needle from the final desired location. With just one 15 gauge needle being used, the incision can be as small as 2 mm to allow the needle to enter. Having conducted over 20 insertions in the dermis phantom for testing and validation, the success rate of insertion is over 95%. Dr. Sydney Cash, a neurologist at the Massachusetts General Hospital, and a collaborator is currently underway to validate this with cadaver experiments. The barb is quick to produce and takes less than 15 minutes of overall

time. It is reproducible - the same mold can be cleaned and reused for multiple strips. With multiple molds, the process is also easily scalable. Both PEG and 3D printing resin are relatively inexpensive commodities, so the barb does not add on to the cost of producing this device. It is situated very far away from the microchips and even the electrodes, so the possibility of damaging the device during insertion is minimized.

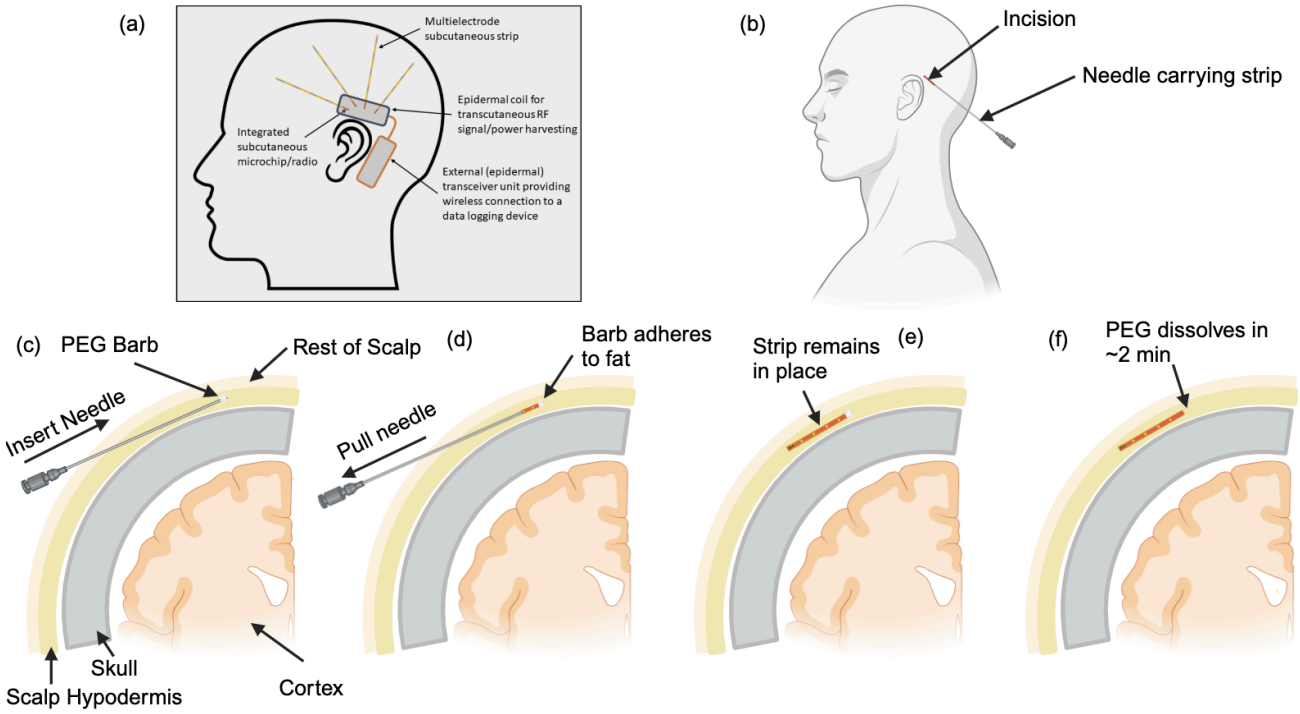


***Figure 7:*** *Insertion Procedure: (a) Concept schematic of entire subdermal EEG system; (b) Location of incision on lateral diagram of adult male head; (c) - (f) Visual representation of how the PEG barb facilitates adhesion during insertion and then dissolves (images not drawn to scale). Note that PI is flexible and length can be modified for greater brain coverage.*

In terms of barb specifics, its dimensions are 1mm x 0.3mm x 0.3mm. This was the minimum thickness required for the PEG to not be brittle. The adhesion of the barb to the PI strip is strong, with 1.2 ± 0.1N force required to remove the barb from the strip. The barbs also stay stable for extended periods of time at room temperature, having been stored for over 30 days. The PEG dissolution starts immediately after the hypodermic needle is extracted and the PEG is

exposed to the bodily environment. Because of the minute amount of PEG used, the total dissolution time is close to 2 minutes. This was approximated using the graphs generated by force testing, shown in Fig. 9b and 9c and Table 2. Immediately after insertion, the force required to pull the strip out was sizable and close to 2N. It is important to note that this was approximated to be 0s but had delays of about 3s manually and 7s using the motorized optical stage (hence first value is lower here) in simply connecting the alligator clip to the strip. The clip could also potentially add compliance forces, which make resultant forces seem smaller and need to be accounted for in future work but was not extremely relevant for our purpose. This dropped down and plateaued to 0.11N around the 2 min mark. The plateau indicates that the PEG dissolved and the force required was simply the baseline force to pull out the strip. The graphs also show an exponential trendline with an $R^2$ of 0.97. This is consistent with the exponential PEG dissolution curve [31].

| **Force using stage (N)** | **Force using hand (N)** | **Time (s)** |
|---|---|---|
| 1.48 | 1.92 | 0 |
| 1.27 | 1.45 | 15 |
| 0.78 | 0.92 | 30 |
| 0.64 | 0.68 | 45 |
| 0.4 | 0.41 | 60 |
| 0.27 | 0.24 | 90 |
| 0.15 | 0.12 | 120 |
| 0.14 | 0.11 | 150 |
| 0.13 | 0.1 | 180 |

***Table 2:*** *Force test results.*

Appendix videos A1-A3 showcase how effective this method is in vitro. The barb allows the strip to be inserted into the dermis phantom. The barbless control gets pushed back into the needle and comes back out with the needle as it is extracted. Going forward, clinical validation from cadaver testing will be crucial to see whether any revisions to the design are needed. Further, this technique of using PEG barbs is not only helpful for our device, but will also be game-changing for any kind of minimally invasive implants that require temporary strength and hardness. These include microelectrodes or microneedles, and so on [32]. The potential for this fabrication technique is wide open.

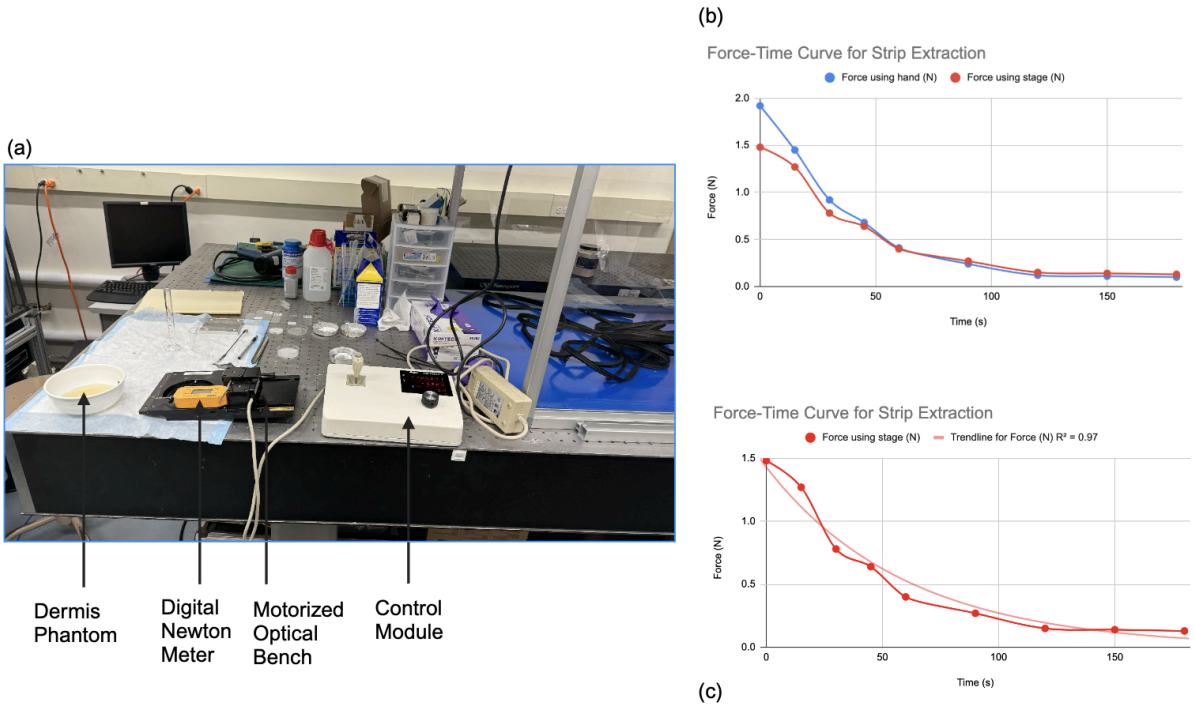


***Figure 8:*** *Force testing: (a) Testing setup with motorized optical bench and newton meter; (b) Force-time curve for manual and automated testing; (c) test results follow an exponential trendline.*

## Data Science

Another clinical consideration in developing a complete subdermal EEG system is to account for the massive amount of data generated by an ultra long term continuous recording. Manually reviewing this data might be time-consuming, expensive, and even prone to error [33]. Data science and machine learning methods have long been used to automate the process of seizure detection and serve as clinician's aids. In this thesis, I build on existing work in the field by using a tree-based algorithm, XGBoost, on a highly used open-source dataset to understand which features are of paramount importance. By reducing the total number of features a model has to work with, I reduce the computation time considerably without compromising on the performance of the model. The entire workflow is shown in Fig. 9.

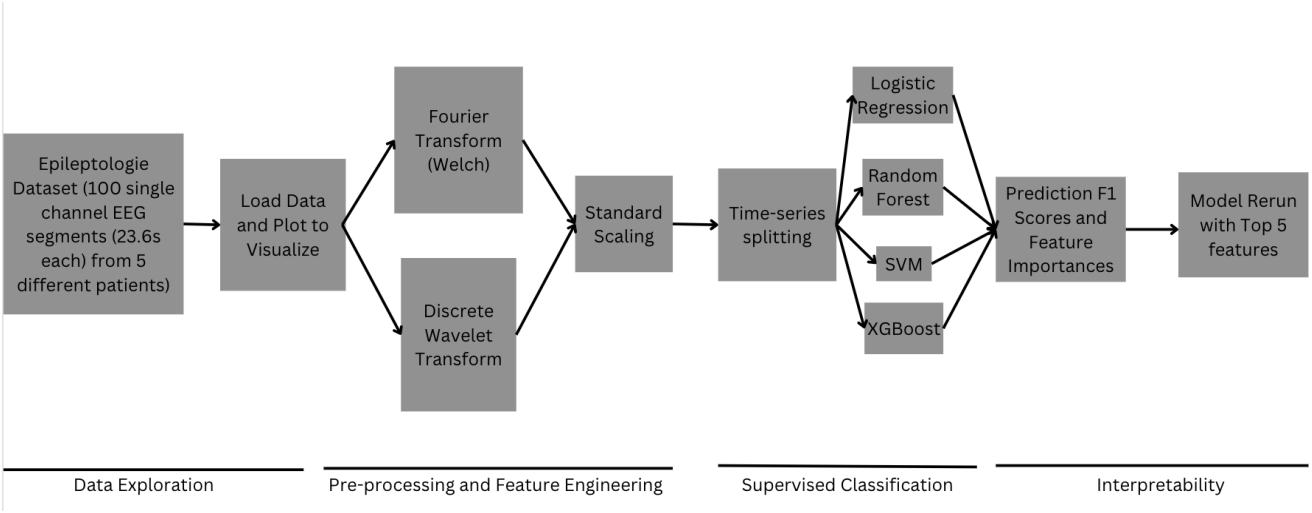


***Figure 9:*** *Flowchart for EEG Seizure Detection ML Algorithm.*

## 3.1 Methods

*Dataset:* Publicly available data was used for this thesis, serving as proxy until our subdermal device is ready to use clinically. The dataset was obtained from Bonn University and is commonly known in the literature as the Epileptologie Dataset [19]. Previous work has seen

multiple models including SVMs, KNNs, ANNs, and random forest be applied to the dataset with high performance [25] [26] [34]. The dataset has five different folders marked A-E, each consisting of 100 single channel EEG segments of 23.6 seconds duration. These segments were selected and cut out from continuous multichannel EEG recordings after visual inspection for artifacts, e.g., due to muscle activity or eye movements [35]. Folders A and B consisted of scalp EEG recordings from 5 healthy volunteers in eyes open and eyes closed states respectively. Folders C, D, and E consisted of EEG recordings from pre-surgical diagnosis of 5 patients. All 5 of these patients underwent surgery and resection of one of the hippocampal formations and achieved complete seizure control. Therefore, these patients had correctly identified epileptogenic zones. Folders C and D contained seizure-free activity (inter-ictal recordings). Folder D had these recordings from the epileptogenic zone and folder C from the opposite hemisphere of the brain. Data in folder E was only seizure activity. All recordings took place from the same 128-channel amplifier system, using an average common reference. The data was digitized using a 12 bit analog-to-digital converter at a sampling frequency of 173.61 Hz. Band-pass filter settings were 0.53– 40 Hz (12 dB/oct.). For this work, only sets C, D, and E were used like in [36], comprising a total of 118 minutes worth of recordings.

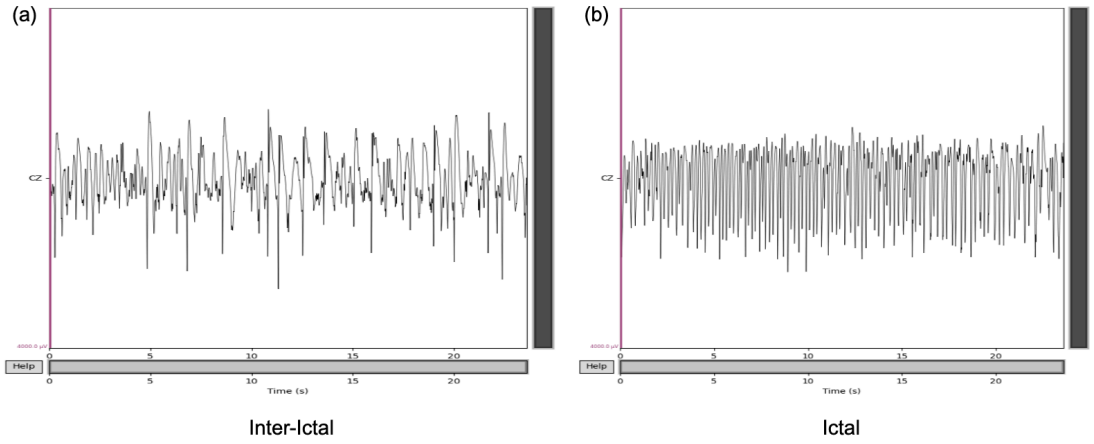


***Figure 10:*** *(a) Sample baseline recording from dataset; (b) Sample seizure recording from dataset*

*Exploratory Data Analysis (EDA):* EDA forms the core of any machine learning pipeline and extensive EDA was performed here to understand what the data looked like and meant. The dataset contained 200 inter-ictal or "baseline" recordings, and 100 ictal or "seizure" recordings. These are shown in Fig. 10. Fig. 11 shows visualizations of a few sample recordings from each folder used. The dataset was not particularly imbalanced, and therefore, no over-sampling or under-sampling methods needed to be applied.

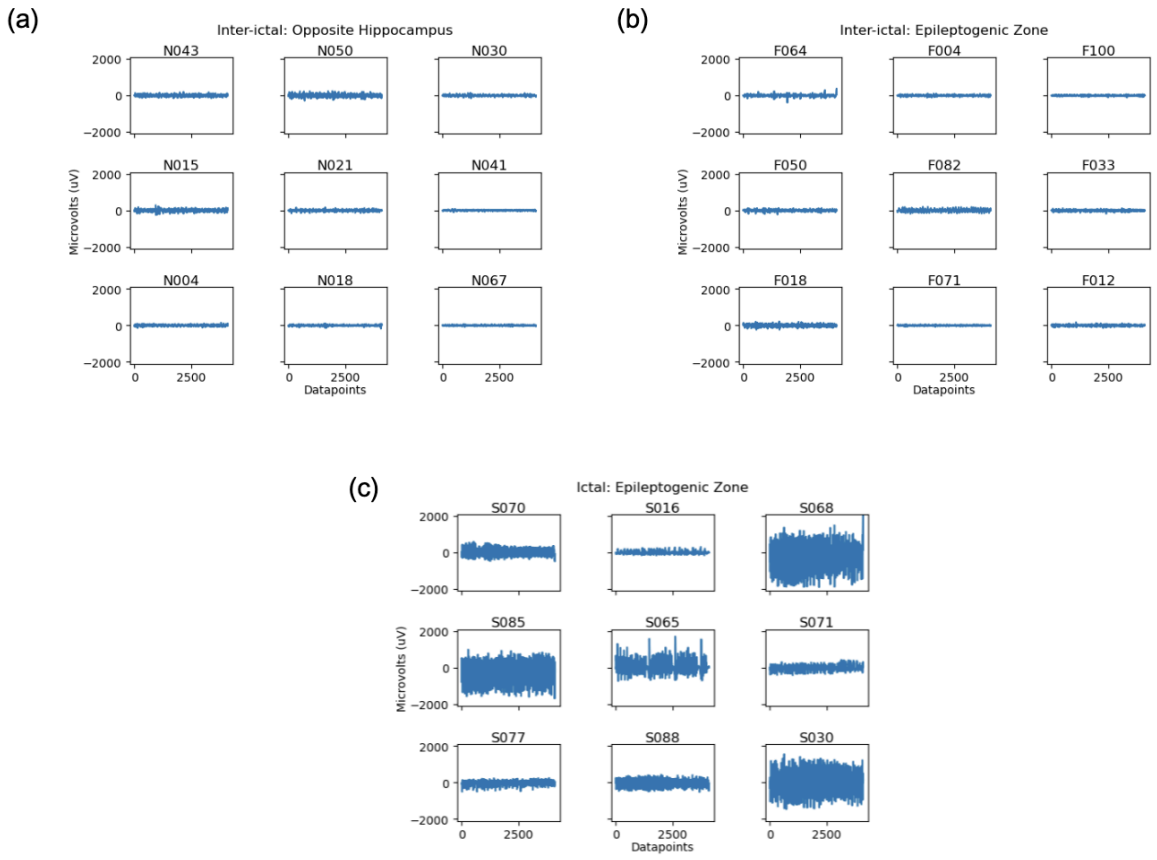


***Figure 11:*** *(a) Sample recordings from folder C; (b) Sample recordings from folder D; (c) Sample recordings from folder E*

*Feature Extraction:* In a complex time-series dataset like this one, feature extraction becomes the most important part of the pipeline. There are dimensions of time, frequency, power, phase, and space. Time is simply how the recorded signal changes amplitude across multiple

sequential samples. Frequency refers to the speed (or the number of cycles per second) of oscillations in the signal, and can be represented in hertz (Hz). Power is the amount of energy in a frequency band, as measured by the squared oscillation amplitude. Phase is the position of an oscillation at a given time point, as measured in radians or degrees [37]. Space refers to the locations of the electrodes on the scalp but in this case with a single channel recording, we do not have to worry about that. Rhythmic brain activity contains multiple overlapping frequencies that can be separated through signal-processing techniques. These are typically grouped into bands of delta (2-4Hz), theta (4-8Hz), alpha (8-12Hz), beta (15-30Hz), and gamma (>30Hz). Each band is reflective of neurobiological mechanisms of brain oscillations and is also associated with separate cognitive functions [38]. Recent work has suggested that high frequency oscillations (HFO) might be most relevant to seizure detection [39]. It has been a hotly contested topic as to what features to extract but for our purposes, we use a standard fourier transform (FT) and discrete wavelet transform (DWT). FT is the transformation of the data from the time domain to the frequency domain by projecting it onto sinusoidal basis functions [40]. Specifically, I use Short-time Fourier transformation's (STFT), which windows the EEG signal and applies a fast Fourier transformation to each data frame. The Welch method is used, which is a spectral density estimation method that calculates a periodogram for windowed sections of data. Overlapping segments are windowed, as this helps mitigate the loss of information at the edges of the time window, with a discrete Fourier transform applied to calculate the periodogram. Data is squared and each periodogram averaged to reduce the variance of each power measure. SciPy is used to extract the power spectral density. Therefore, I obtain the mean power in each of the 5 frequency bands and the ratio of the power of the low frequency bands (delta, theta, and alpha) to the high frequency bands (beta and gamma), giving me a total of 6 features. Next, a DWT is used.

Wavelets can be used to analyze time series with nonstationary power at different frequency bands [41]. The Daubechies 4 wavelet (db4) is the most commonly used wavelet for EEG data as it smooths the frequency filtering enough to characterize the EEG, but is also computationally efficient [42]. The data was decimated into the 6 frequency bins, labeled D1: 43.40 - 86.805 Hz (Gamma), D2: 21.7 - 43.40 Hz (Beta/Gamma), D3: 10.85 - 21.7 Hz (Beta), D4: 5.43 - 10.85 Hz (Alpha), D5: 2.71 - 5.43 Hz (Theta), and D6: 1.36 - 2.71 Hz (Delta). A scalogram to visualize the DWT is shown in Fig. 12. From this, I extract "LSWT": the log-sum energy of the subband coefficients, "mean": average power of the wavelet coefficients in each sub-band, "mean_abs": mean of the absolute values of the coefficients in each sub-band, "std": Standard deviation of the coefficients in each sub-band, and "ratio": ratio of the absolute mean values of adjacent sub-bands. This gives me another 30 features, bringing the grand total to 36 features for the model to analyze. It is important to note that the novelty of this work does not lie in feature engineering. These are all methods used widely before [43].

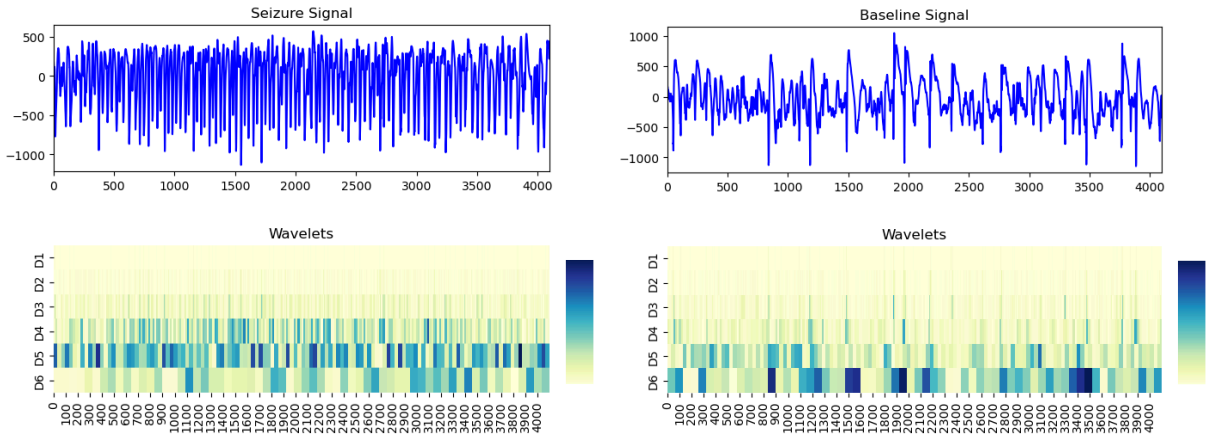


***Figure 12:*** *Scalogram to visualize discrete wavelets for a sample seizure and baseline recording.*

*Models:* A simple train_test_split was used to split the data into a standard 60:20:20 training: validation: testing split. All numerical features were standard scaled. A logistic regression, random forest, support vector classifier, and XGBoost model were trained. For the

evaluation metric, the f_beta score with a standard beta value of 1 was chosen over accuracy to place more emphasis on precision and recall, i.e., the false positives and false negatives, since they are more important for clinical deployment. Eq. 1 denotes the formula to calculate the F1 score.

$$\text{F1 Score} = \frac{TP}{TP + \frac{1}{2}(FP + FN)} \quad \textbf{Eq. 1}$$

Here, TP denotes true positives, FP denotes false positives, and FN denotes false negatives. Various hyperparameters for each model to account for over and underfitting. These hyperparameters, along with the best ones, and the corresponding validation scores are summarized in Table 3. To account for uncertainties due to splitting and due to non-deterministic machine learning (ML) methods, I looped over 5 different random states and collected the mean and standard deviation of the F1 score.

| **Model Name** | **Hyperparameters to Tune** | **Best Parameters** | **Validation Score** |
|---|---|---|---|
| XGBoost | "reg_alpha": [0e0, 1e-2, 1e-1, 1e0, 1e1, 1e2], "reg_lambda": [0e0, 1e-2, 1e-1, 1e0, 1e1, 1e2], "max_depth": [1,3,10,30,100], | {'colsample_bytree': 0.9, 'learning_rate': 0.03, 'max_depth': 1, 'missing': nan, 'n_estimators': 10000, 'reg_alpha': 0.0, 'reg_lambda': 0.0, 'seed': 0, 'subsample': 0.66} | 0.969 |
| Logistic Regression | penalty': ['l1', 'l2', 'elasticnet'], 'C': [0.001, 0.01, 0.1, 1, 10], 'l1_ratio': [0.1, 0.5, 0.9] | {'penalty': 'l1', 'l1_ratio': 0.1, 'C': 0.001} | 1.0 |
| Random Forest | n_estimators': [3, 5, 7, 10, 50], 'max_depth': [1, 3, 5, 10, 20] | {'n_estimators': 10, 'max_depth': 1} | 1.0 |
| SVC | C': [0.1, 1, 10], 'kernel': ['linear', 'rbf', 'poly'], 'gamma': np.logspace(-1,2,5) | {'kernel': 'linear', 'gamma': 0.1, 'C': 0.1} | 1.0 |

***Table 3:*** *Tuning Hyperparameters.*

### 3.2 Results and Discussion

The baseline F1 score was calculated by assigning the minority class for all predictions and came out to be 0.456 ± 0.040. All models performed multiple standard deviations above the baseline score. The test scores are summarized in Table 4 and visualized in Fig. 13. All models hovered around a 0.96 F1 score, consistent with previous literature. The total computational time for the CPU and system was 1 hour 25 minutes and 54 seconds, with the wall time being 11 min and 29 seconds. A normalized confusion matrix was plotted to inspect the model further (Fig. 14). The high false negative rate is a bit concerning, which is why this can only be a clinician's aid and not a replacement.

| **Model Name** | **Mean Test Score** | **Std Test Score** |
|---|---|---|
| XGBoost | 0.963 | 0.035 |
| Logistic Regression | 0.968 | 0.019 |
| Random Forest | 0.956 | 0.027 |
| SVC | 0.968 | 0.019 |
| Baseline | 0.456 | 0.040 |

***Table 4:*** *Summary of test scores for all models vs. baseline.*

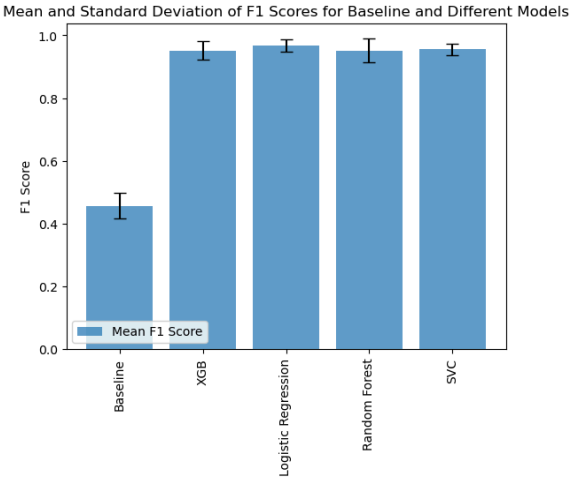


***Figure 13:*** *Summary of test scores for all models vs. baseline.*

To find out the top 5 features, I looked at global feature importances under different metrics: Weight - Number of times a feature appears in trees, Gain - Average gain of the feature when used in trees, Cover - Relative quantity of observations concerned by a feature, Total Gain - Total gain of the feature when used in trees, and Total Cover - Total coverage of the feature when used in trees. This is plotted in Fig. 15. I then calculated SHAP values. Global SHAP feature importance uses SHAP values to measure the average impact of each feature across all instances. This is plotted in Fig. 16. Local SHAP values, on the other hand, look at how the prediction of an individual data point is affected by features. This is shown in Fig. 17 where certain features push the prediction closer to 1 for a seizure data point (Fig. 17a) and certain features push it closer to 0 for a baseline data point (Fig. 17b).

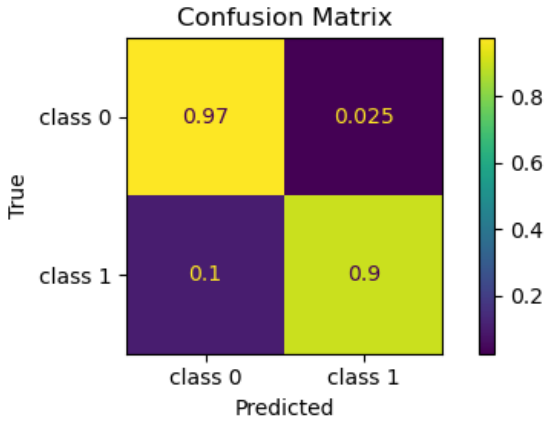


***Figure 14:*** *Normalized confusion matrix of predicted values from XGBoost model.*

None of these feature importances can solely describe the top 5 features. The global feature importance metrics are provided directly by the XGBoost algorithm and therefore, quick and easy to obtain. But they are tree-based and might not capture linear relationships well. Global SHAP feature importances account for interactions between features and provides a unified measure of feature importance. But they are computationally very expensive for large datasets. Local SHAP only looks at individual data points. While all these feature importance

metrics have a different way of obtaining data, they all ultimately lead to us knowing which features are causing the model to behave in a certain way and contributing to predictions. They all increase interpretability of the ML algorithm. The top features remain pretty consistent - ratio of the gamma and gamma/beta discrete wavelet powers, the mean absolute gamma/beta and beta power, the alpha power standard deviation, and the welch power spectral density for the alpha band - even though their rankings might differ from metric to metric. This remains consistent with literature observations that the high frequency bands are key to detecting seizures.

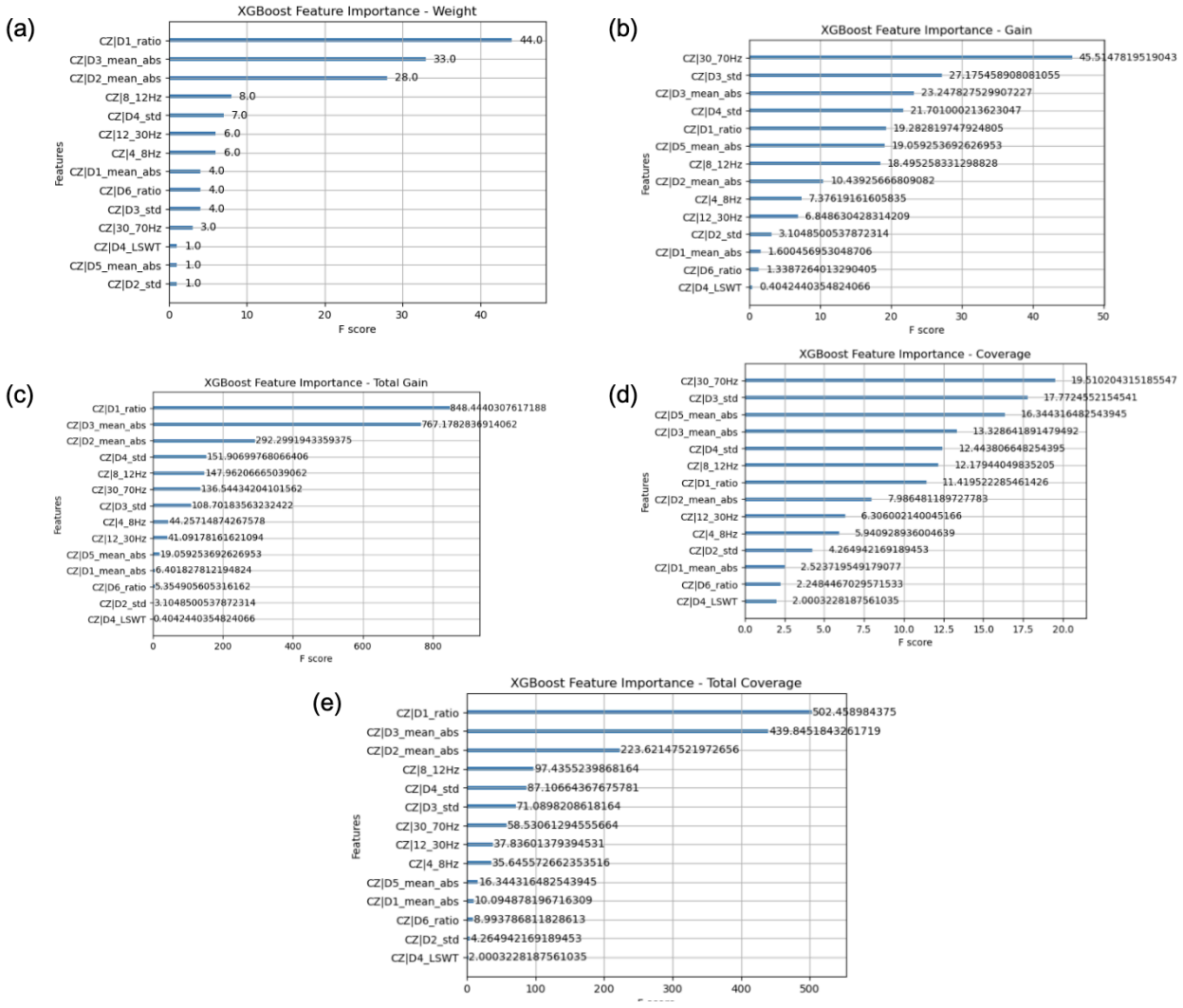


***Figure 15:*** *Global feature importances based on (a) Weight; (b) Gain; (c) Total Gain; (d) Cover; (e) Total Cover.*

All models were then rerun with training on only the top 5 features. The test scores are summarized in Table 5 and visualized in Fig. 18. As is evident, the F1 scores and model performance still remains above 0.95 but the total computation time for the CPU and system is brought down to 44 minutes and 1 second, and the wall time brought down to 5 minutes and 58 seconds. This denotes a 53% decrease in system time and a 48% decrease in wall time. This will be instrumental going ahead when the datasets get big enough.

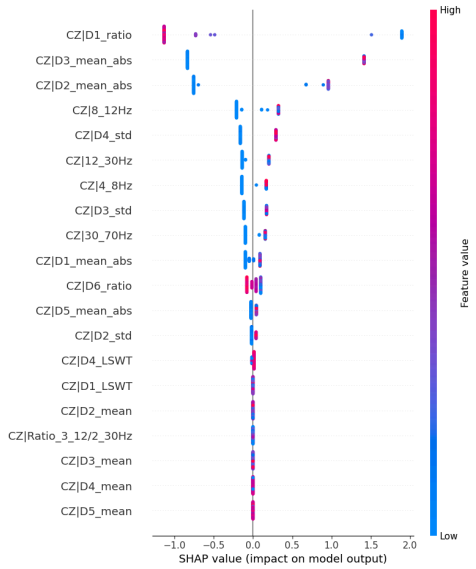


***Figure 16:*** *Global feature importances according to SHAP values.*

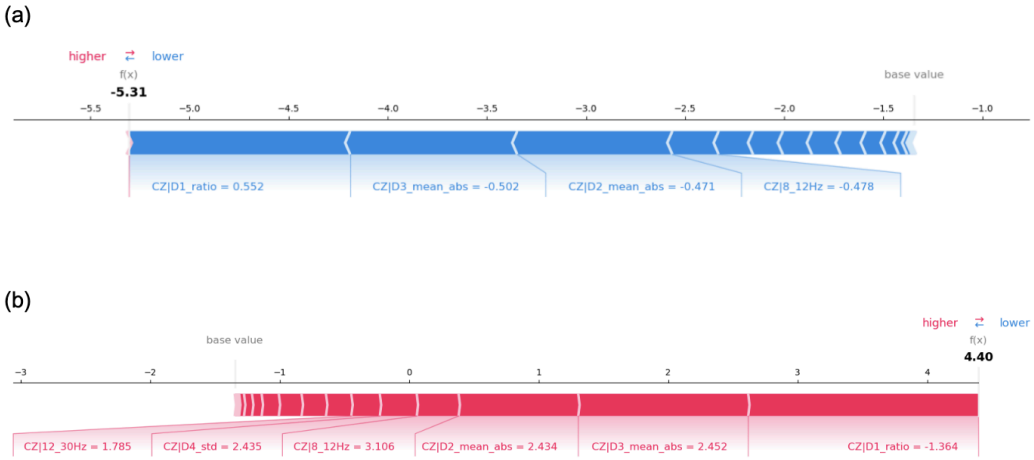


***Figure 17:*** *Local feature importances according to SHAP values for (a) Baseline and; (b) Seizure data point.*

| Model Name | Mean Test Score | Std Test Score |
|---|---|---|
| XGBoost | 0.952 | 0.030 |
| Logistic Regression | 0.967 | 0.019 |
| Random Forest | 0.952 | 0.038 |
| SVC | 0.955 | 0.018 |
| Baseline | 0.456 | 0.040 |

***Table 5:*** *Summary of test scores for all models vs. baseline with only top 5 features.*

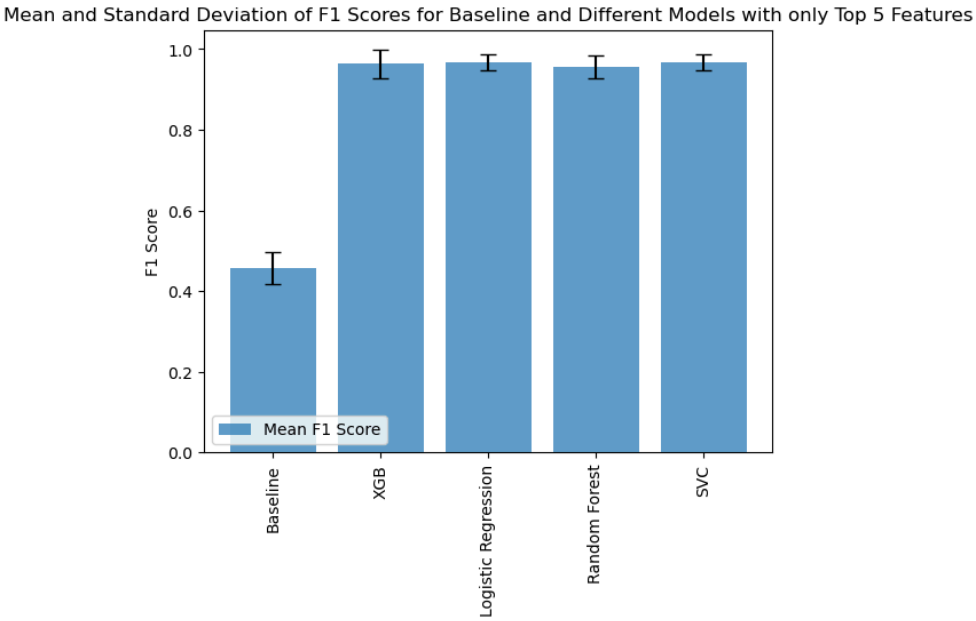


***Figure 18:*** *Summary of test scores for all models vs. baseline with only top 5 features.*

These results do have to be taken with a grain of salt because the dataset here was too small with only 2 hours of data and defined seizure activity. In reality the data is highly imbalanced with only a few short ictal intervals and large inter-ictals, so oversampling techniques have to be used. Further, these were single channel recordings and the code gets much more complicated when one has to account for data from 20 electrodes. This is also, until now, only a seizure detection method. What would be more useful and an avenue of future work is a seizure prediction method. Notwithstanding, this does serve as a proof of concept that feature

importances can be used to significantly decrease the computation time without compromising on model performance. Further, since the training and testing data were from the same pool of patients, this simulation remained true to clinically relevant conditions. This will be highly helpful for all continuous monitoring devices generating large amounts of data, including our subdermal EEG device.

**Conclusion and Future Directions**

The work of this thesis successfully builds on the lab's efforts to produce a minimally invasive, chronic wireless subdermal EEG system for long term use. I provide an easy, quick, and efficient insertion technique by cleverly using bioresorbable PEG microstructures to temporarily increase the strength of our polyimide subdermal strip. Force testing in-vitro indicated that this method is a significant improvement upon existing techniques. Further, I build an entire machine learning pipeline from scratch, extracting feature importances to reduce computation time of automated seizure detection methods by over 50%. Both these achievements go beyond our EEG device and can be used on a broader scale for various chronic monitoring implants.

There is, of course, a lot of potential for future research in the field. The PEG insertion technique must be validated beyond in-vitro phantoms to cadavers and even live volunteers. Multiple different designs for the shape of the barb can also be tested to identify if some work better than the existing design. Some work is also required to add an ergonomic handle to the hypodermic needle to make it easier for clinicians to use. On the data science front, the algorithms must be validated with a much larger dataset to see the implications of reducing features on performance and they should shift focus from simply detection to prediction as well.

Despite limitations, this thesis does provide essential tools for the clinical applicability of chronic, minimally invasive monitoring systems and helps further research in the field of EEG and neural monitoring.

**References**

[1] Tyner, F. S., & Knott, J. R. (1983). *Fundamentals of EEG Technology: Basic concepts and methods* (Vol. 1). Lippincott Williams & Wilkins.

[2] Teplan, M. (2002). Fundamentals of EEG measurement. *Measurement science review*, *2*(2), 1-11.

[3] Duncan, J. S., Sander, J. W., Sisodiya, S. M., & Walker, M. C. (2006). Adult epilepsy. *The Lancet*, *367*(9516), 1087-1100.

[4] Tatum, W. O., Rubboli, G., Kaplan, P. W., Mirsatari, S. M., Radhakrishnan, K., Gloss, D., ... & Beniczky, S. (2018). Clinical utility of EEG in diagnosing and monitoring epilepsy in adults. *Clinical Neurophysiology*, *129*(5), 1056-1082.

[5] Selvitelli, M. F., Walker, L. M., Schomer, D. L., & Chang, B. S. (2010). The relationship of interictal epileptiform discharges to clinical epilepsy severity: a study of routine electroencephalograms and review of the literature. *Journal of Clinical Neurophysiology*, *27*(2), 87-92.

[6] Pathmanathan, J., Kjaer, T. W., Cole, A. J., Delanty, N., Surges, R., & Duun-Henriksen, J. (2022). Expert perspective: who may benefit most from the new ultra long-term subcutaneous EEG monitoring?. *Frontiers in Neurology*, *12*, 817733.

[7] Askamp, J., & Van Putten, M. J. (2014). Mobile EEG in epilepsy. *International journal of psychophysiology*, *91*(1), 30-35.

[8] Nagahama, Y., Schmitt, A. J., Nakagawa, D., Vesole, A. S., Kamm, J., Kovach, C. K., ... & Kawasaki, H. (2018). Intracranial EEG for seizure focus localization: evolving techniques, outcomes, complications, and utility of combining surface and depth electrodes. *Journal of neurosurgery*, *130*(4), 1180-1192.

[9] Parvizi, J., & Kastner, S. (2018). Promises and limitations of human intracranial electroencephalography. *Nature neuroscience*, *21*(4), 474-483.

[10] Lee, A. H., Lee, J., Leung, V., Cash, S., & Nurmikko, A. (2023, October). Minimally Invasive Subdermal Wireless EEG Sensor Arrays for Home Monitoring of Epilepsy. In *2023 IEEE Biomedical Circuits and Systems Conference (BioCAS)* (pp. 1-5). IEEE.

[11] Duun-Henriksen, J., Kjaer, T. W., Looney, D., Atkins, M. D., Sørensen, J. A., Rose, M., ... & Juhl, C. B. (2015). EEG signal quality of a subcutaneous recording system compared to standard surface electrodes. *Journal of Sensors*, *2015*.

[12] Viana, P. F., Duun‐Henriksen, J., Glasstëter, M., Dümpelmann, M., Nurse, E. S., Martins, I. P., ... & Richardson, M. P. (2021). 230 days of ultra long‐term subcutaneous EEG: seizure cycle analysis and comparison to patient diary. *Annals of clinical and translational neurology*, *8*(1), 288-293.

[13] Benovitski, Y. B., Lai, A., McGowan, C. C., Burns, O., Maxim, V., Nayagam, D. A. X., ... & Williams, C. E. (2017). Ring and peg electrodes for minimally-Invasive and long-term sub-scalp EEG recordings. *Epilepsy Research*, *135*, 29-37.

[14] Lee, J., Leung, V., Lee, A. H., Huang, J., Asbeck, P., Mercier, P. P., ... & Nurmikko, A. (2021). Neural recording and stimulation using wireless networks of microimplants. *Nature Electronics*, *4*(8), 604-614.

[15] Uneeg Medical. (2022). *Introducing needle: Instructions for use*. Allerød, Denmark.

[16] Shoeb, A. H., & Guttag, J. V. (2010). Application of machine learning to epileptic seizure detection. In *Proceedings of the 27th international conference on machine learning (ICML-10)* (pp. 975-982).

[17] Goldberger, A. L., Amaral, L. A., Glass, L., Hausdorff, J. M., Ivanov, P. C., Mark, R. G., ... & Stanley, H. E. (2000). PhysioBank, PhysioToolkit, and PhysioNet: components of a new research resource for complex physiologic signals. *circulation*, *101*(23), e215-e220.

[18] Freiburg seizure prediction project. Freiburg, Germany. http://epilepsy.uni-freiburg.de/freiburg-seizure-prediction-project/eeg-database (2003)

[19] Andrzejak, R. G., Lehnertz, K., Mormann, F., Rieke, C., David, P., & Elger, C. E. (2001). Indications of nonlinear deterministic and finite-dimensional structures in time series of brain electrical activity: Dependence on recording region and brain state. *Physical Review E*, *64*(6), 061907.

[20] Herwig, U., Satrapi, P., & Schönfeldt-Lecuona, C. (2003). Using the international 10-20 EEG system for positioning of transcranial magnetic stimulation. *Brain topography*, *16*, 95-99.

[21] Siddiqui, M. K., Morales-Menendez, R., Huang, X., & Hussain, N. (2020). A review of epileptic seizure detection using machine learning classifiers. *Brain informatics*, *7*(1), 5.

[22] Temko, A., Thomas, E., Marnane, W., Lightbody, G., & Boylan, G. (2011). EEG-based neonatal seizure detection with support vector machines. *Clinical Neurophysiology*, *122*(3), 464-473.

[23] Webber, W. R. S., Lesser, R. P., Richardson, R. T., & Wilson, K. (1996). An approach to seizure detection using an artificial neural network (ANN). *Electroencephalography and clinical Neurophysiology*, *98*(4), 250-272.

[24] DeVries, Z., Locke, E., Hoda, M., Moravek, D., Phan, K., Stratton, A., ... & Phan, P. (2021). Using a national surgical database to predict complications following posterior lumbar surgery and comparing the area under the curve and F1-score for the assessment of prognostic capability. *The spine journal*, *21*(7), 1135-1142.

[25] Song, Y., & Liò, P. (2010). A new approach for epileptic seizure detection: sample entropy based feature extraction and extreme learning machine. *Journal of Biomedical Science and Engineering*, *3*(06), 556.

[26] Tzallas, A. T., Tsipouras, M. G., & Fotiadis, D. I. (2007). Automatic seizure detection based on time-frequency analysis and artificial neural networks. *Computational intelligence and neuroscience*, *2007*.

[27] Siddiqui, M. K., Islam, M. Z., & Kabir, M. A. (2017). Analyzing performance of classification techniques in detecting epileptic seizure. In *Advanced Data Mining and Applications: 13th International Conference, ADMA 2017, Singapore, November 5–6, 2017, Proceedings 13* (pp. 386-398). Springer International Publishing.

[28] Bertossi, D., Botti, G., Gualdi, A., Fundarò, P., Nocini, R., Pirayesh, A., & van der Lei, B. (2019). Effectiveness, longevity, and complications of facelift by barbed suture insertion. *Aesthetic surgery journal*, *39*(3), 241-247.

[29] Bender, M., Plachetka, U., Ran, J., Fuchs, A., Vratzov, B., Kurz, H., ... & Lindner, F. (2004). High resolution lithography with PDMS molds. *Journal of Vacuum Science & Technology B: Microelectronics and Nanometer Structures Processing, Measurement, and Phenomena*, *22*(6), 3229-3232.

[30] Chen, A. I., Balter, M. L., Chen, M. I., Gross, D., Alam, S. K., Maguire, T. J., & Yarmush, M. L. (2016). Multilayered tissue mimicking skin and vessel phantoms with tunable mechanical, optical, and acoustic properties. *Medical physics*, *43*(6Part1), 3117-3131.

[31] Corrigan, O. I., Murphy, C. A., & Timoney, R. P. (1979). Dissolution properties of polyethylene glycols and polyethylene glycol-drug systems. *International Journal of Pharmaceutics*, *4*(1), 67-74.

[32] Ko, P. T., Lee, I. C., Chen, M. C., & Tsai, S. W. (2015). Polymer microneedles fabricated from PCL and PCL/PEG blends for transdermal delivery of hydrophilic compounds. *Journal of the Taiwan Institute of Chemical Engineers*, *51*, 1-8.

[33] Varsavsky, A., Mareels, I., & Cook, M. (2011). *Epileptic seizures and the EEG: measurement, models, detection and prediction* (p. 370). Taylor & Francis.

[34] Mursalin, M., Islam, S. S., Noman, M. K., & Al-Jumaily, A. A. (2019). Epileptic seizure classification using statistical sampling and a novel feature selection algorithm. *arXiv preprint arXiv:1902.09962*.

[35] Andrzejak, R. G., Lehnertz, K., Mormann, F., Rieke, C., David, P., & Elger, C. E. (2001). Indications of nonlinear deterministic and finite-dimensional structures in time series of brain electrical activity: Dependence on recording region and brain state. *Physical Review E*, *64*(6), 061907.

[36] Subasi, A., Kevric, J., & Abdullah Canbaz, M. (2019). Epileptic seizure detection using hybrid machine learning methods. *Neural Computing and Applications*, *31*, 317-325.

[37] Cohen, M. X. (2014). Fluctuations in oscillation frequency control spike timing and coordinate neural networks. *Journal of Neuroscience*, *34*(27), 8988-8998.

[38] Başar, E. (2004). Macrodynamics of electrical activity in the whole brain. *International Journal of Bifurcation and Chaos*, *14*(02), 363-381.

[39] Jacobs, J., & Zijlmans, M. (2020). HFO to measure seizure propensity and improve prognostication in patients with epilepsy. *Epilepsy Currents*, *20*(6), 338-347.

[40] Kıymık, M. K., Güler, İ., Dizibüyük, A., & Akın, M. (2005). Comparison of STFT and wavelet transform methods in determining epileptic seizure activity in EEG signals for real-time application. *Computers in biology and medicine*, *35*(7), 603-616.

[41] Sakkalis, V., Zervakis, M., & Micheloyannis, S. (2006). Significant EEG features involved in mathematical reasoning: evidence from wavelet analysis. *Brain Topography*, *19*, 53-60.

[42] Omidvar, M., Zahedi, A., & Bakhshi, H. (2021). EEG signal processing for epilepsy seizure detection using 5-level Db4 discrete wavelet transform, GA-based feature selection and ANN/SVM classifiers. *Journal of ambient intelligence and humanized computing*, *12*(11), 10395-10403.

[43] Dave, E. (2020). *Seizure-Detection-Tutorials: Pre-Processing & Feature Engineering* [Jupyter notebook]. GitHub. https://github.com/Eldave93/Seizure-Detection-Tutorials/blob/master/02.%20Pre-Processing%20%26%20Feature%20Engineering.ipynb

**Appendix A: Links to Videos**

A1: Insertion of PI strip into dermis phantom with PEG barb:

https://drive.google.com/file/d/1H25BeGEGUcw7Tiigt8WSPj-Zm5Qbza74/view?usp=sharing

A2: Insertion of bare PI strip into dermis phantom:

https://drive.google.com/file/d/1tB2wZSYa2aBxx5qxKLNcRDqKWB6m9bKQ/view?usp=sharing

A3: Extraction of PI strip with PEG barb 15 minutes post-insertion:

https://drive.google.com/file/d/1EmsKqGSgepcdsyEHxVQkkD9hZshxGzFm/view?usp=sharing

A4: Force testing using automated optical bench setup:

https://drive.google.com/file/d/1RgR8apAEPlpVkaLnAHEkVCHtT3bFQH0U/view?usp=sharing

**Appendix B: Code Snippets**

```
import xgboost

def xgb_model(X_train, Y_train, X_CV, y_CV, X_test, y_test, verbose=1):
    # make into row vectors to avoid an obnoxious sklearn/xgb warning
    Y_train = np.reshape(np.array(Y_train), (1, -1)).ravel()
    y_CV = np.reshape(np.array(y_CV), (1, -1)).ravel()
    y_test = np.reshape(np.array(y_test), (1, -1)).ravel()
    XGB = xgboost.XGBClassifier()
    # find the best parameter set
    param_grid = {
                "learning_rate": [0.03],
                "n_estimators": [10000],
                "seed": [0],
                "reg_alpha": [0e0, 1e-2, 1e-1, 1e0, 1e1, 1e2],
                "reg_lambda": [0e0, 1e-2, 1e-1, 1e0, 1e1, 1e2],
                "missing": [np.nan],
                "max_depth": [1,3,10,30,100],
                "colsample_bytree": [0.9],
                "subsample": [0.66]
    }
    pg = ParameterGrid(param_grid)
    scores = np.zeros(len(pg))
```

```
for i in range(len(pg)):
    if verbose >= 5:
        print("Param set " + str(i + 1) + " / " + str(len(pg)))
    params = pg[i]
    XGB.set_params(**params)
    eval_set = [(X_CV, y_CV)]
    XGB.fit(X_train, Y_train,
            early_stopping_rounds=50, eval_set=eval_set, verbose=False)  # with early stopping
    y_CV_pred = XGB.predict(X_CV)
    scores[i] = f1_score(y_CV, y_CV_pred)
best_params = np.array(pg)[scores == np.max(scores)]
if verbose >= 4:
    print('Test set max score and best parameters are:')
    print(np.max(scores))
    print(best_params)
# test the model on the test set with the best parameter set
XGB.set_params(**best_params[0])
XGB.fit(X_train, Y_train,
        early_stopping_rounds=50, eval_set=eval_set, verbose=False)
y_test_pred = XGB.predict(X_test)
if verbose >= 1:
    print('The XGB F1 score is:', f1_score(y_test, y_test_pred))
if verbose >= 2:
```

```
        print('The predictions are:')
        print(y_test_pred)
    if verbose >= 3:
        print("Feature importances:")
        print(XGB.feature_importances_)
    return f1_score(y_test, y_test_pred), y_test_pred, XGB.feature_importances_, XGB


# Interpretability
f1, y_test_pred, feature_importances, model = xgb_model(df_train, y_train, df_CV, y_CV,
df_test, y_test, verbose=5)
cm = confusion_matrix(y_test, y_test_pred, normalize='true')
disp = ConfusionMatrixDisplay(cm,display_labels=['class 0', 'class 1'])
fig, ax = plt.subplots(figsize=(5,3))
disp.plot(ax=ax)
plt.title('Confusion Matrix')
plt.xlabel('Predicted')
plt.ylabel('True')
plt.tight_layout()
plt.show()
result = permutation_importance(model, df_test, y_test)
top_indices = np.argsort(result.importances_mean)
plt.figure(figsize=(10, 6))
```

```
plt.boxplot(result.importances[top_indices].T, vert=False, labels=feature_names[top_indices],
widths=0.7)
plt.xlabel('Feature Importance')
plt.title('Feature Importances (Permutation Importance)')
plt.show()
plot_importance(model, importance_type='weight', title='XGBoost Feature Importance -
Weight')
plt.show()
plot_importance(model, importance_type='gain', title='XGBoost Feature Importance - Gain')
plt.show()
plot_importance(model, importance_type='cover', title='XGBoost Feature Importance -
Coverage')
plt.show()
plot_importance(model, importance_type='total_gain', title='XGBoost Feature Importance -
Total Gain')
plt.show()
plot_importance(model, importance_type='total_cover', title='XGBoost Feature Importance -
Total Coverage')
plt.show()
shap.initjs()
explainer = shap.TreeExplainer(model)
shap_values = explainer.shap_values(df_test)
shap.summary_plot(shap_values, df_test,feature_names = feature_names)
```

```
indices = [0, 1, 2, 3, 4]
for id in indices:
    shap.force_plot(explainer.expected_value, shap_values[id, :], features=df_test.iloc[id, :],
feature_names=feature_names, matplotlib=True)
indices = [0, 1, 2, 3, 4]
for id in indices:
    # Extract the feature values for the specific instance
    feature_values = df_test.iloc[id, :].copy()
    # Round numeric feature values to three significant digits
    for col in feature_values.index:
        if isinstance(feature_values[col], (int, float)):  # check if the value is numeric
            feature_values[col] = round(feature_values[col], 3)
    # Generate SHAP force plot with formatted feature values
    shap.force_plot(
        explainer.expected_value,
        shap_values[id, :],
        features=feature_values,
        feature_names=feature_names,
        matplotlib=True
    )
    plt.show()
```

```
model_filename = 'best_model.joblib'
joblib.dump(model, model_filename)
# Save the predictions
predictions_df = pd.DataFrame({
    'True_Labels': y_test,
    'Predicted_Labels': y_test_pred
})
predictions_filename = 'predictions.csv'
predictions_df.to_csv(predictions_filename, index=False)
```